Relaxation Dynamics in Oblate Spherical Rolling Robots

Micah J. Oevermann and Robert O. Ambrose

***Abstract*— Spherical robots rolling on flat ground often exhibit a wobbling motion that, at higher speeds, can escalate into end-over-end flipping. This paper identifies the fundamental dynamic cause of this instability: a relaxation effect analogous to the Intermediate Axis Theorem. Rotating bodies with oblate inertial profiles under dissipative loads tend to reorient toward rotation about their major moment of inertia, leading to the observed wobbling in spherical robots. While relaxation dynamics are well-studied in satellites and asteroids, they have not been previously applied to rolling systems with contact constraints. We extend these methods to constrained spherical robots, derive the governing dynamics, and validate them through experiments with an empty shell and a reduced pendulum on flat ground and in water. Results show that translational rolling constraints are the primary driver of instability; however, appropriate design and actuation strategies can mitigate this effect. This work bridges the fields of satellite dynamics theory and ground robotics, providing new insights into the stability of high-speed rolling robots.**

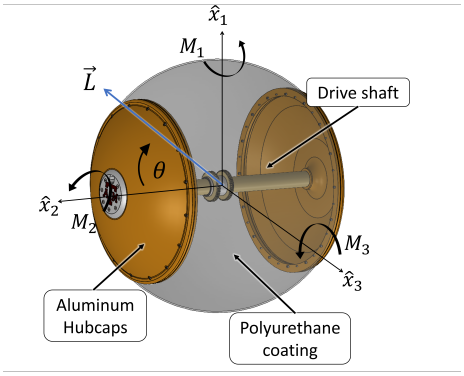

Fig. 1. Diagram of a robot shell's body frame with angular momentum vector, applied moment components, and relaxation angle between the momentum and minimum inertia axis $\hat{x}_2$

I. Introduction

The rotational motion of free-flying tri-axial objects is a unique and well-studied phenomenon. The most famous case is the Dzhanibekov effect, also known as the tennis racket or Intermediate Axis theorem. Where an object rotating about its intermediate moment of inertia will tend to flip from one side to the other [1]. Additionally, free-flying rotating objects under some form of dissipative load will eventually settle into rotation about their major moment of inertia to minimize kinetic energy. Cigar-shaped satellites, such as Explorer I, were initially set spinning about their minor moment of inertia; however, energy dissipated by structural vibrations in its antenna caused the satellite to attempt to settle into rotations about its major inertial axis. Study of this dissipative relaxation toward maximal-inertia rotation effect has had a lasting impact on spin-stabilized satellite design and Eulerian mechanics theory [2]. This is also recognized by astronomers studying spinning asteroids. In that field, the use of a "relaxation angle" or the angle of the angular momentum expressed in the body frame relative to an inertia axis is used to classify asteroid spin states and study their dynamics [3]. The techniques and intuition for studying complex rotations of free-flying objects could also be applied to the study of spherical robots; however, the theory has yet to be extended to rolling objects.

Spherical robots have gained popularity over the past few years [4]. Generally, they are designed with an outer shell and an inner mechanism to generate rolling torque. Figure 1 shows an example schematic of a shell from a spherical robot that is typically driven by a pendulum; this shell is inflatable with a soft polyurethane coating as its primary rolling surface [5]. It would be reasonable to assume that a rotating object constrained to roll on a surface would display characteristics of the Intermediate Axis Theorem, especially if that object (or robot) is of non-uniform inertia. However, studies on spherical robots have either not addressed these effects directly or ignored them. The next couple of paragraphs will discuss several spherical robots and comment on whether they used a full 3D model or approximated a sphere as two cylinders for a decoupled approach. Since the inertia profile of a body is the driving factor behind the Dzhanibekov effect, the inertia tensors of the outer shells of their robots, as reported in their papers, will also be provided.

Arif et al. employed a flywheel with a decoupled model to reduce oscillations and achieve higher speeds [6]; however, they did not report the shell's inertial profile. Asiri developed a full dynamic model with a control scheme based on centripetal forces, but observed no unexpected motion in their experiments. Their robot had an almost uniform, slightly oblate profile [7]. Belzile used a fully coupled model and stated that the inertia was uniform, although photographs in their paper show a shaft across the sphere, which would alter the final inertia [8]. Feng also presented a full model, but simplified it enough to reduce it to an uncoupled system. While no inertia values were provided, their kinetic energy formulation (eq. 21 in [9]) implies unequal inertias.

B. Li adopted a Lagrangian formulation with kinematic constraints embedded directly into the derivation. They briefly acknowledged a wobbling behavior during turns but did not analyze it further, focusing instead on their novel

**Research supported by the Texas A&M Chancellor's Research Initiative and matching funds from the Texas Governor's University Research Initiative.

Authors are with Texas A&M University, College Station TX, US

jumping mechanism [10]. As a result, no internal inertial profiles were reported. Wang followed a decoupled approach similar to that discussed in Chapter 2 and therefore reported only one inertia [11]. Ylikorpi introduced a soft-shell robot similar to the one shown in Figure 1, featuring an inflatable outer shell. Their model considered only one plane of motion but noted that the inertia could vary with inflation pressure and shell geometry [12].

Schroll constructed a full 3D model and observed what he coined as a "nutation instability" where the robot would excessively wobble at high speeds until it flipped hubcap to hubcap [13]. Singhal constructed a model similar to Schroll's, but arrived at the opposite conclusion that these effects would die out at higher speeds, although the claim was not supported by experiments [14].

A summary of these studies is given in Table I. For those works that do provide inertial values, the axes have been redefined so that the middle inertia (I_2) is aligned with the robot's primary intended rolling direction, similar to Figure 1.

TABLE I
REPORTED INERTIAL PROFILES OF OUTER SHELLS

Model Type	Inertial Profile $[kg-m^2]$ $[I_1,\ I_2,\ I_3]$
Uncoupled [6]	Not Given
Uncoupled [9]	non-uniform via eq. 21
Uncoupled [11]	$[\text{N/A}, 0.888, \text{N/A}]$
Uncoupled [12]	$[\text{N/A}, (5.85-7.18)e^{-2}, \text{N/A}]$
Coupled [7]	$[2.65, 2.57, 2.65]e^{-2}$
Coupled [8]	$[0.25, 0.25, 0.25]$
Coupled [10]	Not given
Coupled [13]	$[0.25, 0.15, 0.25]$
Coupled [14]	Uniform Inertia
This Paper	$[1.04, 0.64, 1.04]$

From the list of inertial profiles in the table, it is clear that the possible inertial effects of the various robots' rotating outer shells have not been adequately studied or have been ignored entirely by using an uncoupled model. Developing a thorough understanding of the effect can influence the proper inertial profile necessary for rolling robots at higher speeds. The remainder of this paper will review useful dynamic analysis techniques used when studying the Intermediate Axis theorem. Then, it will extend those methods by applying constraints used to model rolling objects and provide a discussion on the differences between the two cases. Additional experiments and numerical studies will be presented to further explore the relationship between a rolling inertial object and its natural rolling stability.

II. DYNAMIC ANALYSIS OF ROTATING BODIES SUPPLEMENTED WITH RELAXATION DYNAMICS

This section reviews two modeling paradigms: one derived from Euler's rotation equations and another from relaxation dynamics as presented by Likins in [2]. Both models will use the notation illustrated in Figure 1. Where the body frame axes are given by $\hat{x}_i$, and the net moments and angular velocities about the axes are given by M_i or ω_i for the i^{th} axis. Euler's equations use the individual components, while the relaxation dynamics will use the angle θ between the angular momentum vector. This vector is defined in equation (1), and similar statements can be made for the vectors of $\vec{M}$ and $\vec{\omega}$.

$$\vec{L} = I\vec{\omega} = I_1\omega_1\hat{x}_1 + I_2\omega_2\hat{x}_2 + I_3\omega_3\hat{x}_3 \tag{1}$$

A. Euler Dynamics of a Rotating Body

The motion of a spinning body under the influence of external moments is described by Euler's equations, which are presented below. Here I is the inertia tensor of the rotating body.

$$I\dot{\vec{\omega}} + \vec{\omega} \times I\vec{\omega} = \vec{M} \tag{2}$$

However, from Table I most spherical robots are not tri-axial inertially; rather, they are ordered by $I_1 = I_3 > I_2$. Inertial profiles of this form are commonly referred to as "oblate" objects.

Consider a case where M represents a satellite under uniform structural damping, so that it takes the form of (3). Here C is a diagonal matrix of positive damping constants.

$$M = -C\omega \tag{3}$$

To examine the stability of free rotations with equation (2), assume constant rotation about ω_2 with small perturbations in ω_1 and ω_3 as δ_1 and δ_3 respectively. Ignoring $\delta_1\delta_3$ terms as negligible yields the dynamics in the form of $\dot{x} = A(\omega)x$, shown in (4).

$$\begin{pmatrix}\dot{\delta}_1\\ \dot{\omega}_2\\ \dot{\delta}_3\end{pmatrix} = I^{-1}\begin{bmatrix}-C & 0 & (I_2-I_3)\omega_2\\ 0 & -C & 0\\ (I_1-I_2)\omega_2 & 0 & -C\end{bmatrix}\begin{pmatrix}\delta_1\\ \omega_2\\ \delta_3\end{pmatrix} \tag{4}$$

So the eigenvalues of this system are given by

$$\lambda_1 = -C \tag{5a}$$

$$\lambda_{2,3} = -C \pm |\omega_2|\sqrt{(I_2-I_3)(I_1-I_2)} \tag{5b}$$

If the inertias are distinct and ordered ($I_3 > I_2 > I_1$), the radical will stay real so that one of the eigenvalues could become positive for large enough speeds of ω_2. This is the essence of the Intermediate Axis Theorem.

However, if the inertias are oblate ($I_3 = I_1 > I_2$), then (5b). takes the form of (6). So that the troublesome radical term becomes imaginary. Yet, the real parts are still negative, so rotations about that axis are stable, albeit with some decaying harmonics.

$$\lambda_{2,3} = -C \pm i|\omega_2|\sqrt{(I_2-I_1)^2} \tag{6}$$

Thus, while free oblate bodies appear stable, the inclusion of a relaxation angle shifts the stability picture dramatically.

B. Relaxation Dynamics of a Damped Oblate Body

Defining a relaxation angle can give insight into the evolution of a body's rotational profile over time. In astrophysics, this angle is typically defined as the angle between the body's angular momentum vector and its greatest moment of inertia [3]. Most spherical robots roll about their minimum moment of inertia as shown in Table I. This section will redefine the relaxation angle with respect to that axis, rather than the maximum axis. The angle, angular momentum vector, and shell body frame are shown in Figure 1. When defined in this way, if the robot is rolling forward or driving straight, then $\vec{L}$ is aligned purely along $\hat{x}_2$, and the angle is zero. Likewise, if the shell is flipping end over end, then the vector would lie in the $\hat{x}_1 - \hat{x}_3$ plane, and the angle would be 90°. A schematic demonstrating these characteristics is shown in Figure 2.

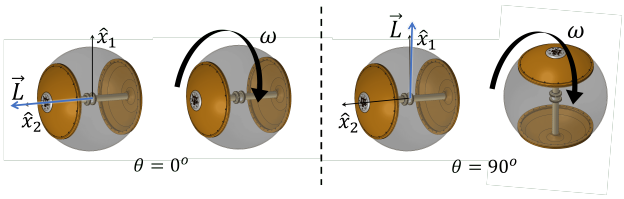

Fig. 2. A robot shell in two edge case relaxation states

The angle is calculated directly with (7).

$$\cos(\theta) = \frac{I_2\omega_2}{||L||} \tag{7}$$

Where $||L||$ is the norm of the angular momentum, given by (8).

$$||L||^2 = \omega^T I^2 \omega = I_1^2(\omega_1^2 + \omega_3^2) + I_2^2\omega_2^2 \tag{8}$$

With the rotational kinetic energy given by (9).

$$2T = \omega^T I\omega = I_1(\omega_1^2 + \omega_3^2) + I_2\omega_2^2 \tag{9}$$

The relaxation angle θ can be expressed in terms of T and $||L||$ following an identical procedure shown by Likins in Section IV of [2]. The resulting relationship is expressed in (10) for our definition of the angle.

$$\cos^2(\theta) = \frac{I_2(2I_1T - ||L||^2)}{||L||^2(I_1 - I_2)} \tag{10}$$

If the change in momentum is small, then (10) can be differentiated directly to (11) as shown in Likins.

$$\dot{\theta} = \frac{2}{\sin(2\theta)} \frac{I_1 I_2}{||L||^2(I_2 - I_1)} \dot{T} \tag{11}$$

This equation is the *relaxation dynamics* of a rotating body. It is a tool to study the evolution of a rotating oblate body's rotational profile over time.

The behavior of equation (11) can be studied by separating it into three terms and determining their signs: the sinusoidal fraction, the inertia ratio, and the rate of change of angular kinetic energy. The first part, the sinusoid ratio, is positive within the quadrant between $\hat{x}_2$ and the $\hat{x}_1 - \hat{x}_3$ plane. For the inertia ratio, $||L||^2$ is always positive. Therefore, the sign of this term depends on the ordering of the inertias. For spherical robots, $I_1 > I_2$, so this term is negative. That leaves the stability of (11) down to the rate of rotational kinetic energy change, $\dot{T}$. This can be expressed in terms of the applied moment to the body using equations (2) and (9) and shown in (12).

$$\begin{aligned} 2\dot{T} &= \dot{\omega}^T I\omega + \omega^T I\dot{\omega} \\ \dot{T} &= \omega^T I\dot{\omega} \\ &= \omega^T(M - \omega \times (I\omega)) \\ \dot{T} &= \omega^T M \end{aligned} \tag{12}$$

As with the eigenvalue analysis, apply uniform damping to the system to mimic the structural dissipation of a satellite, as shown in equation (3). So the relaxation dynamics become

$$\dot{\theta} = \frac{2}{\sin(2\theta)} \frac{I_1 I_2}{||L||^2(I_2 - I_1)}(-\omega^T C\omega) \tag{13}$$

The term $-\omega^T C\omega$ is negative definite for all non-zero ω. The positive sine term, negative inertia ratio, and negative dissipation terms net a positive sign for $\dot{\theta}$. Therefore, a rotating floating body under dissipation will experience a reduction in angular magnitude, but a shift in net rotational direction towards the $\hat{x}_1 - \hat{x}_2$ plane. As a robot's shell rotates under some dissipative load, it will shift to flip hubcap-to-hubcap, illustrated by Figure 2.

C. Comparing Responses of Rotation and Relaxation Dynamics

Figures 3 and 4 show results from numerically integrating (2) for both free and uniformly damped rotations, as defined by (3). The middle and right of the figures contain the calculation of the relaxation angle with equation (7) and rotational kinetic energy as defined by (9). The simulations used the inertia for this paper from Table I and $c_i = 0.05$.

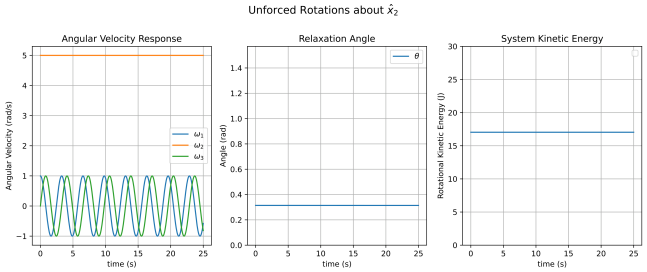

Fig. 3. Free rotations of oblate body in a stable wobbling motion

Figure 3 displays behaviors for a floating and rotating oblate body discussed in the previous sections, ($M = 0$). One of the eigenvalues is zero under zero damping, while the others exhibit sinusoidal behavior. The relaxation angle is constant because there is no change in energy, but it is not

zero since not all of the angular momentum is aligned with $\hat{x}_2$.

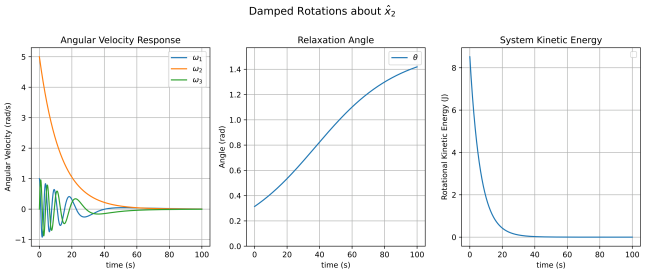

Fig. 4. Free body stable, but damped system drifts toward relaxation

Figure 4 shows the same system as above, but now uniformly damped in all axes. The system is damped, so the velocities and the kinetic energy decay. However, the relaxation angle increases, indicating that as it slows, the body will eventually transition from rotating about the drive axis to flipping from hubcap-to-hubcap before coming to a stop.

Since the momentum angle encodes a direction, this effect could also be shown, although less elegantly, by defining a set of orientation states through eigenvalue analysis. This approach avoids the complexities that arise with Euler-angle singularities or quaternion math. Although there is still a dynamic singularity when operating at very slow speeds when $||L|| \to 0$.

III. Relaxation Dynamics for Rolling Oblate Bodies

The previous section reviewed the behavior of free-flying objects in two cases: free rotations and under uniform damping. Since spherical robots are not satellites, the theory will need to be constrained to the rolling case. This section will bridge the gap between the previous section by applying appropriate constraints for a sphere rolling on an inclined surface.

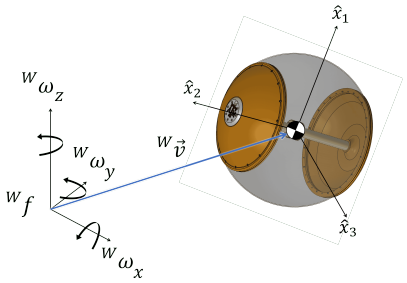

Fig. 5. The robot shell located in the world frame

A. Rolling constraint and contact Jacobian

Figure 5 illustrates the motion of a robot's shell within the world frame. For the remainder of this section, values expressed in the world or inertial frame will be preceded with a superscript $^w(\cdot)$. Values expressed in the body frame will have no superscript to remain consistent with the previous sections. When a sphere rolls without slipping on a plane, the translational velocity $^w v$ is related to its rotational velocity in the world frame by equation (14), where R is the nominal outer shell radius.

$$^w v = \bar{R}\ ^w\omega \tag{14}$$

where

$$\bar{R} = \begin{bmatrix} 0 & R & 0 \\ -R & 0 & 0 \\ 0 & 0 & 0 \end{bmatrix},$$

Defining $^w R_b$ as a transform from the body frame to the world frame, express (14) in the form of (15) with respect to the body angular velocities.

$$^w v = \bar{R}\,^w R_b\,\omega \tag{15}$$

Define the generalized velocity vector

$$\dot{q} = \begin{bmatrix} ^w v \\ \\ \omega \end{bmatrix}. \tag{16}$$

The constraints can be written compactly as a contact Jacobian in (17), where eye_3 represents the identity matrix of size three. This notation is introduced to keep it distinct from the body inertia tensor I.

$$J(q)\dot{q} = 0, \qquad J(q)^T = \begin{bmatrix} \text{eye}_3 \\ -(\bar{R}\,^w R_b)^T \end{bmatrix} \tag{17}$$

B. Constrained dynamics

The equations of motion with constraints then take the form

$$A(q)\ddot{q} + H(q,\dot{q}) = F + J^T\lambda, \tag{18}$$

with a block-diagonal mass matrix

$$A = \begin{bmatrix} m\ \text{eye}_3 & 0 \\ \\ 0 & I \end{bmatrix}, \tag{19}$$

where m is the mass and I is the inertia tensor in the body frame of the robots shell.

Splitting into linear and angular components in (20). Here m is the shell mass, $^w F_v$ are applied linear forces in the world frame such as gravity, with other angular terms consistent with (2).

$$m\,^w\dot{v} = {}^w F_v + \lambda \tag{20a}$$

$$I\dot{\omega} + \omega \times (I\omega) = M - (\bar{R}\,^w R_b)^T\lambda. \tag{20b}$$

From the linear block, solve for λ directly with:

$$\lambda = m\,^w\dot{v} - {}^w F_v \tag{21}$$

Substituting into the angular block gives the reduced rotational dynamics:

$$I\dot{\omega} + \omega \times (I\omega) = M - (\bar{R}\,^w R_b)^T(m\,^w\dot{v} - {}^w F_v) \tag{22}$$

C. Expression for angular kinetic energy rate

Redefine the kinetic energy rate following a similar procedure from equation (12).

$$\dot{T} = \omega^T M - \omega^T (\bar{R}\,{}^w R_b)^T (m\,{}^w\dot{v} - {}^w F_v) \tag{23}$$

Recall the rolling constraint, Eq. (15) we obtain

$${}^w v^T {}^w\dot{v} = \omega^T (\bar{R}\,{}^w R_b)^T {}^w\dot{v}.$$

Therefore,

$$-\omega^T (\bar{R}\,{}^w R_b)^T m\,{}^w\dot{v} = -m\,{}^w v^T {}^w\dot{v} = -\frac{d}{dt}\left(\frac{1}{2} m\,{}^w v^T {}^w v\right).$$

That reduces down to the rate of change in kinetic energy.

$$-\omega^T (\bar{R}\,{}^w R_b)^T m\,{}^w\dot{v} = -\dot{T}_{trans} \tag{24}$$

where the translational kinetic energy is given below.

$$T_{trans} = \frac{1}{2} m\,{}^w v^T {}^w v \tag{25}$$

In this case (23) can be simplified to (26)

$$\dot{T} = \omega^T M - \dot{T}_{trans} + \omega^T (\bar{R}\,{}^w R_b)^T {}^w F_v \tag{26}$$

This highlights the additional effects rolling introduces on the system's angular kinetic energy. The angular power from the body frame moments remains the same as before, but now includes the energy siphoned to translational rolling motion (which behaves like an additional dissipative term), as well as the work done by linear forces mapped into the system. The relaxation stability of a rolling object is still dependent on a positive sign of $\dot{T}$.

D. Interpreting Linear Forces

If the system is rolling unpowered down a slope and the global coordinate frame and initial body frame are aligned along the angle of the slope, as shown in Figure 6. Then ${}^w R_b = eye_3$ and the only other force doing work on the system through ${}^w F_v$ is gravity, shown in (27) with α as the constant incline angle.

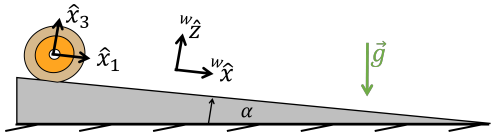

Fig. 6. World frame aligned with object rolling down slope

$${}^w F_v = \begin{pmatrix} mg\sin(\alpha) \\ 0 \\ -mg\cos(\alpha) \end{pmatrix} \tag{27}$$

the final term in (26) can be simplified to

$$\omega^T (\bar{R}\,{}^w R_b)^T {}^w F_v = \omega_2 mgR\sin(\alpha) \tag{28}$$

To study the stability of a rolling object, in this case, the sign of (29) must be positive. Assuming that the soft contact between the polyethylene shell and the concrete can be modeled close enough with the dissipative effect in (3).

$$\dot{T} = -\omega^T C\omega - \dot{T}_{trans} + \omega_2 mgR\sin(\alpha) \tag{29}$$

From equation (29), all variables in the final gravity term are positive and will stay positive as ω_2 increases down the slope. However, as the object accelerates down the ramp, $\dot{T}_{trans}$ will also be positive along with the quadratic damping term. At fast enough speeds, $\dot{T}_{trans}$ and the quadratic damping term will overpower the linear-in-velocity gravity term, resulting in a negative sign for $\dot{T}$. In this case, the system will experience the relaxation effect and flip hubcap-to-hubcap.

This is counterintuitive to our free-flying object scenario. If the relaxation dynamics from (11) are considered without accounting for the translational coupling between the angular and translational components, intuition would assume that the net angular kinetic energy would increase as the system rolls down the slope, stabilizing the system. The next section will support (29) with an experiment with the robot shell.

IV. Shell Rolling Experiments

To verify (29), a series of experiments was conducted with only the robot's shell. A VN-100 IMU was mounted inside the robot's hubcaps to directly measure $\vec{\omega}$. The additional weight was balanced to keep the inertial profile as close to oblate as possible, but only accounted for an additional $0.62kg$ on the total system mass of $17.16kg$. A schematic of this setup is shown in Figure 7. A bare shaft was used in place of a drive mechanism to keep the shell's shape and nominal outer radius of $0.31m$.

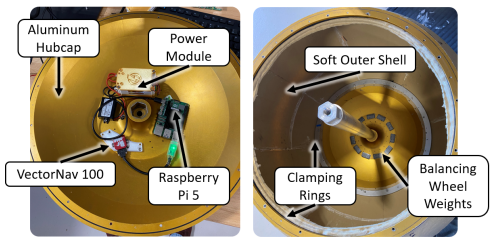

Fig. 7. Instrumentation of Robot Shell

This empty shell was then placed at the top of a slightly sloped concrete slab ($\alpha \approx 2°$), inflated to a set pressure, and allowed to roll down the slope. This allowed for multiple runs with a consistent set of initial conditions since the shell alone has no actuation capabilities. Figure 8 shows screenshots of the shell undergoing the relaxation or nutation instability. As it rolls under the influence of gravity, the hubcaps roll parallel to the viewer, but as it relaxes, they roll hubcap to hubcap. The same effect was shown in Figure 6.

Fig. 8. Screenshots of the shell experiencing a nutation instability, the hubcaps start parallel to the viewer, then shift to perpendicular while maintaining a steady path away

Data from one of the runs is shown on the left of Figure 9 with the relaxation angle and kinetic energy calculated in post-processing. Recall from (11) that the relaxation angle is a function of the angular momentum of the system, so small irregularities from the concrete and shell will affect the net energy of the system in a chaotic way. A third-order Savitzky-Golay filter was employed to remove most of the noise in the angular velocity readings. The kinetic energy decreases towards the end of the tests as the effect of the robot rolling over the mounting interface from soft shell to hard hubcap slows the system.

Fig. 9. Data from a single run of the shell rolling down a slope

To determine if pressure has a significant effect on the relaxation rate, trials were conducted at two main pressure levels. The filtered relaxation angles were used to calculate an average rate of relaxation, determining whether system pressure had a significant effect on the relaxation dynamics. In this testing case, there appears to be no significant relationship between the rate of relaxation and pressure, shown by the linear regression in Figure 10.

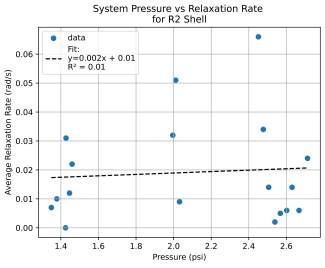

Fig. 10. Relaxation angle drift during shell rolling experiment, showing onset of instability

For similar types of robots, the pressure of the shell had a significant effect on the control system [15]. However, the lack of a noticeable effect here implies that the dissipative effect of the shell might not be the main driver behind the sign of $\dot{T}$ and subsequently the relaxation effect. The next section will utilize various environmental testing cases to relax the kinematic constraints and subsequently $\dot{T}_{trans}$.

V. Rolling Dynamics with Looser Constraints

Adding a pendulum mechanism to the shell enables control over the shell's angular velocities. The bare shaft in the shell from Figure 7 is replaced with a reduced pendulum assembly as shown in Figure 11. Usually, this pendulum allows for actuation in a drive axis $\hat{x}_2$, and a perpendicular steering axis. However, a 3D printed clamp was added to remove motion not about $\hat{x}_2$. This assembly was then tested on flat ground and floating in water, and the body velocities were recorded through an IMU mounted on the pendulum.

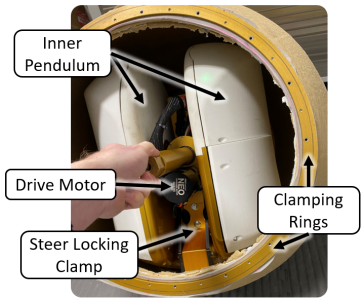

Fig. 11. Locked Steering Clamp

The stability of the relaxation dynamics for the robot rolling on flat ground now needs to include the effects of the pendulum on the system. Assuming that the net moment on the body frame can be separated into $M = M_{pend} + M_{contact}$. Where $M_{contact}$ can be represented by the uniform dissipation from (3), and M_{pend} is the gravity torque brought on by the pendulum reflected into the shell frame, this can be compactly stated in (30) as a function of the shell's position in space ${}^{w}R_b$ and the rotated angle of the pendulum around the driveshaft, θ_d.

$$M_{pend} = f({}^{w}R_b, \theta_d) \tag{30}$$

The stability of the system is still dependent on the sign of the new $\dot{T}$ in (31).

$$\dot{T} = \omega^T M_{pend} - \omega^T C\omega - \dot{T}_{trans} \tag{31}$$

This is not a trivial exercise since the forces of the pendulum depend on its pose with respect to gravity in the world frame and the state angles (${}^{w}R_b$ and θ_d). However, it is possible to choose M_{pend} such that the system is stable at high speeds ([11, 15]). Irresponsible choices can also drive the system unstable; therefore, the sign of $\omega^T M_{pend}$ is arbitrary and can be both positive and negative.

A series of experiments was conducted with the robot in this configuration. For each run, the robot was commanded to track a certain speed in ω_2. While rolling, an IMU attached to the pendulum assembly recorded the shell's body angular velocities. The resulting data and calculated relaxation angles are shown in Figure 12.

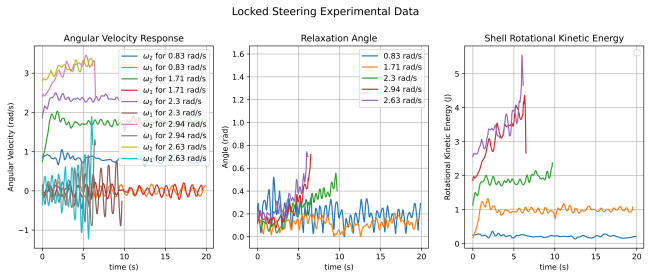

Fig. 12. Relaxation angles of the system rolling at increasing speeds with a reduced pendulum on land

From the data in Figure 12, the restricted pendulum was able to prevent the system from relaxing at slower speeds. So $\dot{T}$ in this situation was negative. However, once speeds start to exceed around 2 radians per second, the system's reduced pendulum will no longer be able to balance the system, and it begins to experience the relaxation effect.

However, when the robot is placed in a similar situation in water, shown in Figure 13, the same pendulum could balance the system at much higher speeds. The resulting relaxation angle is shown in Figure 14.

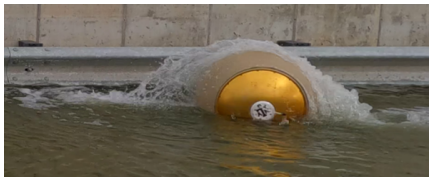

Fig. 13. Robot rolling in water at around 18 rad/s

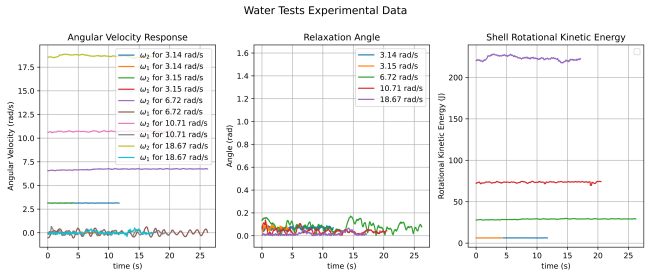

Fig. 14. Relaxation angles of the robot rolling at high speeds on water

Comparing the tests where the robot rolls on flat ground to those on water, the constraints given by equation (14) are no longer valid, as the robot slips significantly more on water than on land. As a result, $\dot{T}_{trans}$ as defined with that equation breaks down. So the pendulum can overcome the additional dissipation effects and does not experience the relaxation effect.

VI. Discussion

Switching to water to overcome the relaxation effect is rarely practical. Robot designers have two options to mitigate this effect in their prototypes: adjust the outer shells' inertial profile or adapt the control scheme.

From (11) and (31), a pendulum-driven system rolling on level ground is unstable. Reversing the shell's inertia profile so that rolling occurs about the major moment of inertia changes the sign of $\dot{\theta}$, naturally stabilizing the motion without altering the control scheme or environment.

When redesigning is not feasible, stabilization can be achieved through control instead. The choice of M in (31) determines the sign of $\dot{\theta}$, making it a useful tuning parameter. This perspective extends to other actuation methods such as flywheels, where θ could be incorporated into an observer-based controller, provided the singularity at rest is appropriately managed.

VII. Conclusion

This paper extends the theory of relaxation dynamics, well established in satellite and asteroid mechanics, to the domain of rolling spherical robots. By analyzing oblate inertial profiles under rolling constraints, we showed that the wobbling and eventual flipping observed in spherical shells are natural consequences of the relaxation effect. The derived equations, supported by experimental trials with varying internal configurations and constraint conditions, demonstrate that translational rolling constraints play a dominant role in driving this instability by acting as an additional dissipation mechanism.

Looking forward, this connection between classical rotational dynamics and constrained robotic motion opens the door to new control approaches. These techniques could be adapted to actively regulate momentum alignment in rolling robots. More broadly, the relaxation framework offers a compact tool for analyzing and predicting stability in mobile rolling platforms where shape, inertia, and ground interaction are tightly coupled.

References

[1] Mark S Ashbaugh, Carmen C Chicone, and Richard H Cushman. "The twisting tennis racket". In: *Journal of Dynamics and Differential Equations* 3 (1991), pp. 67–85.

[2] Peter W Likins. *Effects of energy dissipation on the free body motions of spacecraft*. Tech. rep. Jet Propulsion Laboratory, 1966.

[3] Michael Efroimsky. "Relaxation of wobbling asteroids and comets—theoretical problems, perspectives of experimental observation". In: *Planetary and Space Science* 49.9 (2001), pp. 937–955.

[4] Aminata Diouf et al. "Spherical rolling robots—Design, modeling, and control: A systematic literature review". In: *Robotics and Autonomous Systems* 175 (2024), p. 104657.

[5] Micah Oevermann et al. "Roboball: An all-terrain spherical robot with a pressurized shell". In: *2024 IEEE International Conference on Robotics and Automation (ICRA)*. IEEE. 2024, pp. 13502–13508.

[6] Muhammad Affan Arif et al. “Design of an amphibious spherical robot driven by twin eccentric pendulums with flywheel-based inertial stabilization”. In: *IEEE/ASME Transactions on Mechatronics* 28.5 (2023), pp. 2690–2702.

[7] Samira Asiri et al. “The Design and Development of a Dynamic Model of a Low-Power Consumption, Two-Pendulum Spherical Robot”. In: *IEEE/ASME Transactions on Mechatronics* 24.5 (2019), pp. 2406–2415.

[8] Bruno Belzile and David St-Onge. “ARIES: Cylindrical pendulum actuated explorer sphere”. In: *IEEE/ASME Transactions on Mechatronics* 27.4 (2022), pp. 2142–2150.

[9] Zhaohan Feng and Hanxu Sun. “A high-speed motion control method of pendulum driven spherical robot”. In: *2021 IEEE International Conference on Artificial Intelligence and Computer Applications (ICAICA)*. IEEE. 2021, pp. 1–7.

[10] Bing Li, Qiang Deng, and Zhichao Liu. “A spherical hopping robot for exploration in complex environments”. In: *2009 IEEE International Conference on Robotics and Biomimetics (ROBIO)*. IEEE. 2009, pp. 402–407.

[11] Yixu Wang et al. “Robust servo linear quadratic regulator controller based on state compensation and velocity feedforward of the spherical robot: Theory and experimental verification”. In: *International Journal of Advanced Robotic Systems* 20.2 (2023).

[12] Tomi J Ylikorpi, Aarne J Halme, and Pekka J Forsman. “Dynamic modeling and obstacle-crossing capability of flexible pendulum-driven ball-shaped robots”. In: *Robotics and Autonomous Systems* 87 (2017), pp. 269–280.

[13] Gregory C Schroll et al. “Dynamic model of a spherical robot from first principles”. MA thesis. Colorado State University. Libraries, 2010.

[14] Animesh Singhal et al. “Pendulum actuated spherical robot: dynamic modeling & analysis for wobble & precession”. In: *IFAC-PapersOnLine* 55.22 (2022), pp. 67–72.

[15] Derek J. Pravecek et al. “Empirically Compensated Setpoint Tracking for Spherical Robots With Pressurized Soft-Shells”. In: *IEEE Robotics and Automation Letters* 10.3 (2025), pp. 2136–2143.